npj | climate and atmospheric science

Article

Published in partnership with CECCR at King Abdulaziz University

https://doi.org/10.1038/s41612-026-01324-9

Mechanisms driving altitude- and latitude-dependent air quality variations from high-altitude NO_x emissions

Check for updates

Lucas J. Oh[1], Sebastian D. Eastham[1,2] ✉ & Steven R. H. Barrett[1,3]

The environmental impact of nitrogen oxide (NO_x) emissions varies with emission altitude and latitude. NO_x emissions from subsonic aviation (9-12 km) contribute to net global ozone formation, whereas those from supersonic aircraft (above 14 km) lead to net global ozone depletion. However, the effects of NO_x emission altitude on surface air quality remain understudied. We evaluate how NO_x emissions at different altitudes (8–22 km) and latitudes influence near-surface concentrations of two known air pollutants: ozone and fine particulate matter ($PM_{2.5}$). Using the global chemical transport model GEOS-Chem, we find that NO_x emissions of 1 Tg N yr^{-1} at 8–10 km (30–60°N) increase surface ozone (population-weighted) by 0.52 ppb and surface $PM_{2.5}$ by 35 ng m^{-3}, whereas emissions at 20–22 km reduce surface ozone by 1.73 ppb and increase surface $PM_{2.5}$ by 310 ng m^{-3}; this is nine times the $PM_{2.5}$ increase per unit NO_x from lower-altitude emissions. These effects stem from altitude-dependent mechanisms: at lower altitudes typical of subsonic aviation, NO_x emissions increase upper tropospheric ozone which leads to enhanced surface ozone and nitrate aerosol. However, when emitted at higher altitudes NO_x instead depletes ozone, permitting more ultraviolet light to reach the troposphere which boosts OH production and accelerates production of sulfate aerosol while destroying near-surface ozone. Our findings suggest that NO_x emissions from high-altitude sources, including supersonic aircraft may not only contribute to stratospheric ozone depletion but also cause larger changes (albeit of mixed sign) in surface air quality than subsonic aviation per unit of NO_x emitted.

Emissions of nitrogen oxides (NO_x) impact both global air quality and climate[1–4]. NO_x is emitted from sources including fossil fuel combustion, industrial activities, lightning, and microbial soil processes[5–7] and, through atmospheric reactions, can influence surface concentrations of ozone (O_3) and fine particulate matter ($PM_{2.5}$) and thereby degrade surface air quality[5,8–13].

Studies on the impact of lightning and aviation NO_x emissions on air quality have demonstrated that the altitude and location of emission qualitatively change the magnitude of the effect on air quality[3,6,14–17]. One of the reasons for this sensitivity is that the amount of ozone produced per unit of NO_x emitted is 3–15 times greater at typical aircraft cruise altitudes than at the surface[1,18]. Additionally, in regions with lower NO_x backgrounds, like the Southern Hemisphere, net ozone production per unit NO_x can be over twice as high as in more NO_x-rich regions like Europe[1].

Lightning NO_x, of which 65% is emitted in the tropics between 7 and 11 km and 23% in the Northern extratropic between 3 and 7 km, has been estimated to contribute 0.44 ppb Tg N^{-1} to global surface ozone and 3 ng m^{-3} Tg N^{-1} to $PM_{2.5}$[6,19]. Aviation emissions, with 80% released at cruise altitude (9–12 km), have similarly been estimated to cause a 0.59 ppb Tg N^{-1} increase in global mean surface ozone and a 12 ng m^{-3} Tg N^{-1} increase in surface $PM_{2.5}$[14]. Aggregating globally, 53,100 premature deaths per year due to ozone exposure and 21,200 premature deaths per year due to $PM_{2.5}$ exposure have been attributed to aviation emissions, and almost exclusively due to aviation NO_x released during cruise[14]. Concerns over the near-airport air quality impacts of aviation have led to regulations limiting NO_x emissions per unit of thrust for subsonic aviation[20]. However, these regulations do not account for how the altitude and geographic location of emissions influence their atmospheric impact.

[1]Department of Aeronautics and Astronautics, Massachusetts Institute of Technology, Cambridge, MA, USA. [2]Department of Aeronautics, Imperial College London, London, UK. [3]Department of Engineering, University of Cambridge, Cambridge, UK. ✉e-mail: s.eastham@imperial.ac.uk

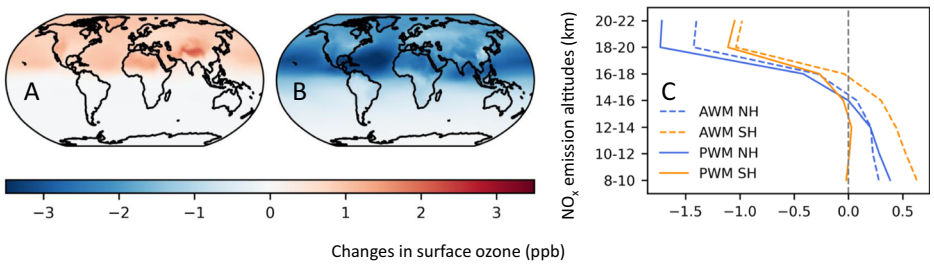


Fig. 1 | Surface ozone responses to NO_x emissions. Changes in global annual mean surface ozone concentrations (ppb) at different NO_x emission altitudes between 30°N and 60°N: **A** 8–10 km and **B** 14–16 km. **C** Changes in weighted mean surface ozone concentrations (ppb) at different NO_x emission altitudes for each hemisphere. Solid lines represent the population-weighted mean (PWM) ozone changes, while dashed lines indicate the area-weighted mean (AWM) ozone changes. Results are shown separately for emissions in the Northern Hemisphere (NH, blue) and Southern Hemisphere (SH, orange). All maps use coastlines from the Natural Earth dataset (public domain) and are rendered using the Cartopy library.

Furthermore, the future distribution of aviation and lightning NO_x emissions may differ from current patterns. Demand for air travel is expected to increase with economic growth in the Southern Hemisphere[21,22]. Projections indicate that by 2050 the aviation growth rate will be 5.35% per year in Africa and 5.1% in Latin America compared to 3.45% in Europe and 3.1% in North America, suggesting a potential shift in the latitudinal distribution of aviation emissions[21]. For lightning NO_x, models already differ in estimates of current-day distribution and intensity[6], and future projections remain uncertain[23,24]. Without a mechanistic understanding of the connection between NO_x emissions location and air quality consequences it is not yet possible to predict what these changes will mean for future global public health.

The understanding of NO_x impacts on surface air quality now also needs to extend to higher altitudes due to the potential reintroduction of supersonic flight. Companies like Boom Supersonic aim to reintroduce supersonic passenger aircraft, leading to new NO_x emissions at higher altitudes. Boom's Overture model proposes a cruise speed of Mach 1.7 and a cruise altitude of 18 km[25]. United Airlines has announced a commercial agreement under which it has the option of purchasing 15–50 Overture aircraft, with the first flights proposed for 2029[26]. NO_x emissions at altitudes of 13–23 km induce ozone depletion[27–34], in contrast to conventional tropospheric aviation NO_x emissions (9–12 km) which promote ozone formation[3,35–37]. Previous study found that increasing cruise altitude from 13 to 23 km changed the net effect on global ozone from +3.3 to −28 DU Tg N^{-1} [31], while studies of subsonic aviation (9–12 km, cruise) have found an increase ranging from 0.46 to 0.90 DU Tg N^{-1}[38–46]. These findings are consistent with results showing an "ozone neutral" altitude for NO_x emissions at around 14 km, below which emissions of NO_x increase ozone and above which they decrease net ozone[47]. It was also shown that the increase in population exposure to ultraviolet radiation due to limited stratospheric ozone depletion may be accompanied by a reduction in surface level ozone, resulting in a potential public health trade-off [48].

Despite this, no study to date has addressed the magnitude and mechanism of the change in surface air quality as a function of the altitude of emission, and this information is urgently needed. In addition to civil aviation, growth in the use of rocket launches, satellite reentry, and potentially even deployment platforms for climate engineering all constitute active or potential sources of NO_x over a range of altitudes which have not previously been considered in air quality assessment.

We address this gap. We use a version of the global chemistry transport model GESO-Chem 11.02 modified to better represent the effects of supersonic emissions[28,49] to simulate emissions of NO_x at different altitudes and latitudes and quantify surface air quality outcomes. By isolating the specific mechanisms behind these changes, we enhance the understanding of higher altitude NO_x emissions' effects and provide support for potential policy actions such as regulating flight paths, emissions standards, and mitigation strategies to minimize environmental impacts on air quality.

Results and discussion

We quantify surface ozone and $PM_{2.5}$ changes from NO_x emission perturbations in 35 different latitude and altitude combinations. For each combination, we emit 3 Tg N yr^{-1} with results then normalized to 1 Tg N yr^{-1} by scaling values by one third. We evaluate global air quality impact using the population-weighted and area-weighted mean changes in concentrations of surface ozone (ppb) and $PM_{2.5}$ (ng m^{-3}). Details are provided in the "Methods" section.

Changes in surface ozone

NO_x emissions at 8–10 km and between 30°N and 60°N (Fig. 1A) lead to surface ozone increases concentrated in the Northern Hemisphere, where the area-weighted mean enhancement is 0.71 ppb over Northern Hemisphere (compared with a global mean of 0.34 ppb). Across the Northern Hemisphere, surface ozone increases with area-weighted mean increases of 0.53 ppb over 0–30°N and 0.91 ppb over both 30–60°N and 60–90°N (Fig. 1A). This increase is greater in high-elevation regions: the Rocky Mountains (area-weighted mean: 1.13 ppb), Greenland (1.07 ppb), the Zagros Mountains (1.06 ppb), and the Tibetan Plateau (1.54 ppb). The Sahara Desert (1.04 ppb), the Arabian Peninsula (0.83 ppb), and oceanic areas (Northern Atlantic: 0.93 ppb) also exhibit greater ozone changes than the Northern Hemisphere average (0.71 ppb). Meanwhile, surface ozone changes are below the Northern Hemisphere average in India (0.39 ppb) and Eastern China (0.55 ppb). Ozone changes over the Eastern United States (0.72 ppb) and Central Europe (0.68 ppb) are comparable to the Northern Hemisphere average. However, when compared to their respective regional mean values (0.86 ppb for the United States and 0.76 ppb for Europe), the changes in the Eastern United States and Central Europe are lower by 0.14 ppb and 0.08 ppb, respectively (see regional definitions in Supplementary Table S1).

The net surface ozone response shifts from an increase to a decrease as the emission altitude rises. Global area-weighted mean surface ozone decreases by 1.40 ppb because of NO_x emissions at 20–22 km and between 30°N and 60°N (Fig. 1B). Over the Northern Hemisphere, the area-weighted mean decrease reaches 2.22 ppb. The geographical pattern is also different, with the greatest changes occurring at low latitude. We find an area-weighted mean decrease of 2.42 ppb over 0–30°N, while 30–60°N and 60–90°N show smaller decreases of 2.07 ppb and 1.90 ppb, respectively (Fig. 1B). We also find that surface ozone reductions are larger over the ocean than over land. For instance, the South Atlantic exhibits a decrease of 3.11 ppb, compared with 2.41 ppb over the Sahara Desert, 2.24 ppb over the Tibetan Plateau, and 1.4 ppb over Eastern China (see "Mechanisms driving surface ozone reduction"). The variation in surface ozone impacts by altitude of NO_x emission is further illustrated (Fig. 1C), which presents population-weighted and area-weighted mean changes of global mean surface ozone as a function of the altitude. Total emissions in each hemisphere are normalized to 1 Tg N yr^{-1}. The Northern Hemisphere mean represents the area-weighted average of three simulations conducted for the latitude bands (Eq-30°N, 30–60°N, and 60–90°N), while the Southern Hemisphere mean represents the area-weighted average of two simulations

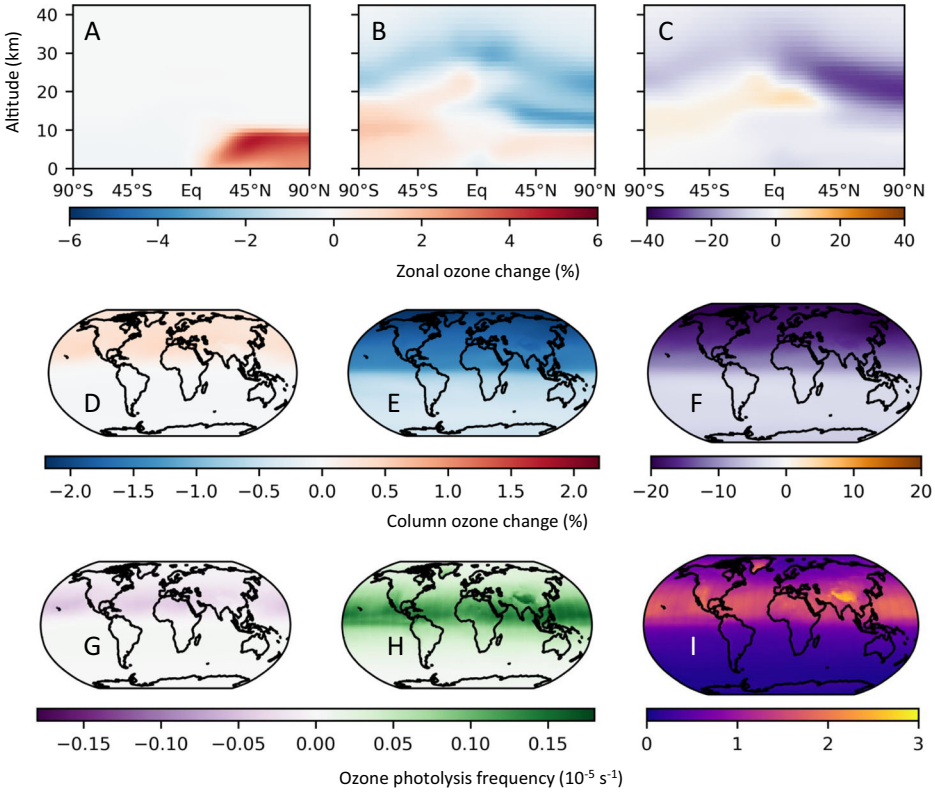


Fig. 2 | Zonally averaged ozone and ozone photolysis frequency response to aviation NO_x emissions at different altitudes. **A**–**C** show the percent change in zonally averaged ozone from emissions at three altitude ranges: **A** 8–10 km, **B** 14–16 km, and **C** 20–22 km, originating between 30°N and 60°N. **D**–**F** present the resulting annual mean changes in column ozone (percent) over the same latitude band for emissions at **D** 8–10 km, **E** 14–16 km, and **F** 20–22 km. **G**–**I** show the corresponding changes in annual mean ozone photolysis frequency ($\times 10^{-5}\,s^{-1}$) over the same latitude band for emissions at **G** 8–10 km, **H** 14–16 km, and **I** 20–22 km.

(Eq-30°S, and 30–90°S) (see Supplementary for details). NO_x emissions above 16 km always reduce global mean surface ozone concentrations, regardless of the location of emissions or the weighted-mean calculation method. NO_x emissions below 14 km instead increase surface ozone, with the only exception being the population-weighted mean change due to emissions in the Southern Hemisphere.

The sign of surface ozone change varies with the altitude of NO_x emissions (Fig. 1C), implying different health impacts. It was reported that a 0.8 ppb increase in population-weighted mean surface ozone attributable to aviation emissions can result in approximately 53,100 premature deaths[14]. Our findings indicate that NO_x emissions at 8–10 km (30–60°N) increase the population-weighted mean ozone by 0.52 ppb per 1 Tg N yr^{-1}, whereas NO_x emissions at 20–22 km (30–60°N) decrease it by 1.70 ppb per 1 Tg N yr^{-1} (Fig. 1A, B).

In addition to emissions altitude, we also find differences in impact due to emissions latitude (Fig. 1C). In regions where the surface ozone increases (below 14 km of emissions altitude), the area-weighted mean change is higher due to emissions in the Southern Hemisphere than in the Northern Hemisphere. For NO_x emissions at 8–10 km, the average surface ozone increase is 0.28 ppb Tg N^{-1} for Northern Hemisphere emissions and 0.63 ppb Tg N^{-1} for Southern Hemisphere emissions. For emissions above 16 km, which instead cause a reduction in the surface ozone, the absolute reduction is larger for emissions occurring in the Northern Hemisphere. Northern Hemisphere emissions at 20–22 km decrease surface ozone by 1.40 ppb Tg N^{-1}, while Southern Hemisphere emissions reduce it by 0.98 ppb Tg N^{-1}. These results demonstrate that the surface ozone response depends not only on emission altitude but also on the emissions latitude (see "Impact of NO_x emission latitude on the geographic distribution of surface ozone").

Changes in global ozone

To understand the impact of NO_x emissions on surface ozone, we examine their effect on global ozone at different altitudes. NO_x emissions at 8–10 km between 30°N and 60°N lead to a net ozone increase (Fig. 2A), with the Northern Hemisphere total ozone burden increasing by 0.25% Tg N^{-1}. Below 10 km altitude (i.e., within the troposphere) this increase is greater, at 2.5% Tg N^{-1}. The pattern and magnitude are consistent with prior estimates of the effects of subsonic aviation NO_x, which is mostly emitted in this region[37].

In contrast, emissions at 14–16 km and 20–22 km produce a mixed ozone response, characterized by both production and depletion with net ozone loss in the mid-stratosphere (Fig. 2B, C). Overall, emissions at 14–16 km reduce the Northern Hemisphere total ozone burden by 1.6% Tg N^{-1}, while emissions at 20–22 km lead to a larger decrease of 15% Tg N^{-1}, consistent with prior studies of supersonic aviation NO_x above 20 km[31–34]. Despite the similarity in mixed signals, the latitudinal and vertical structure differs between the 14–16 km and 20–22 km cases (Fig. 2B, C). For example, NO_x emissions at 14-16 km still enhance ozone in the Northern Hemisphere below 10 km by 0.27% Tg N^{-1}, whereas emissions at 20–22 km instead reduce ozone below 10 km by 4.6% Tg N^{-1}. The response of the vertical ozone profile to emissions at 14–16 km across the tropics and Northern Hemisphere shows an intermediate mix of these two patterns. Descending from the emissions altitude, stratospheric ozone (specifically above 10 km) decreases by 1.9% Tg N^{-1}, followed by tropospheric increase (below 10 km) of 0.27% Tg N^{-1}. This tropospheric change also includes mixed signs, with increases in mid-tropospheric ozone but a decrease of 0.16% Tg N^{-1} at the surface (Fig. 2B).

The contrasting effects of lower-altitude NO_x-induced ozone production and higher-altitude NO_x-induced stratospheric ozone depletion are also reflected in changes to total column ozone. Emissions at 8–10 km increase global mean total column ozone by 0.11% Tg N^{-1} (Fig. 2D). In contrast, emissions at 14–16 km and 20–22 km lead to global mean decreases of 1.1% and 9.4% Tg N^{-1}, respectively (Fig. 2E, F). These results are consistent with findings that NO_x emissions below ~13.5 km result in net ozone production, while emissions above this altitude lead to net depletion[47].

Changes in column ozone are known to alter the amount of UV radiation reaching the surface, with potential implications for surface

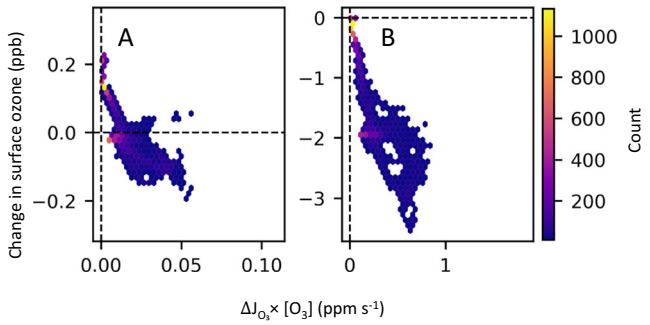


Fig. 3 | Hex bin plot of surface ozone change (ppb, *y*-axis) versus ozone destruction rate (ppm s^{-1}, *x*-axis) for NO$_x$ emissions between 30°N and 60°N. **A** Emissions at 14–16 km, **B** emissions at 20–22 km. Only bins containing at least 10 data points are shown.

photochemistry[48]. We also investigate this mechanism (Fig. 2G, H, I) (see "Mechanisms driving surface ozone reduction").

Mechanisms driving surface ozone enhancement

Studies investigating aviation NO$_x$ impacts on surface ozone have described the mechanism by which subsonic aviation NO$_x$ increases surface ozone through the NO$_x$-O$_x$-VOC cycle[3]. At cruise altitudes of around 9–12 km NO$_x$ emissions drive net ozone formation, which is then transported downward allowing aviation NO$_x$ to contribute to an increase in surface ozone[3,14,36]. This downward transport near 30°N (Fig. 2A) explains the surface ozone enhancement over high-altitude regions like the Rocky Mountains, Tibetan Plateau, and Greenland, where shorter vertical transport distances intensify ozone transport from the upper atmosphere (Fig. 1A). However, it does not explain increases in lower-elevation inland regions like the Sahara Desert and Arabian Peninsula, or over the Atlantic and Pacific Oceans (Fig. 1A).

Previous studies have also suggested that aviation-induced ozone can serve as a sink for surface NO$_x$, thereby reducing surface NO$_x$ concentrations over regions such as Europe[3]. Conversely, these findings imply that background NO$_x$ can act as a chemical sink for ozone transported from higher altitudes. When ozone is transported to these high-NO$_x$ regions, transported ozone reacts with ambient NO$_x$, thereby dampening the surface ozone increase caused by ozone transport from NO$_x$ emissions at 8–10 km. This may explain why some areas at low elevation show greater ozone change. The low background NO$_x$ concentrations (<1 ppb) in the Sahara Desert (10–30°N) and oceans (Eq-30°N) mean that transported ozone can persist longer than in regions with high NO$_x$ backgrounds. The increase in surface ozone due to NO$_x$ emissions between 8 and 14 km can be suppressed in high-NO$_x$ regions. In these same regions, enhanced ozone-NO$_x$ interactions may lead to increased PM$_{2.5}$ concentrations through secondary aerosol formation (see "Changes in surface PM$_{2.5}$").

Our results also support a dampening mechanism by which surface ozone increases are suppressed in regions with high background NO$_x$ concentrations. We examine changes in surface NO$_x$ concentrations resulting from NO$_x$ emissions at 8-10 km over 30–60°N (see Supplementary Fig. S1). Surface NO$_x$ concentrations decrease across nearly all regions due to ozone transported from aloft reacting with ambient NO$_x$ (see Supplementary Fig. S1). The largest decreases occur in high-NO$_x$ regions such as the eastern United States (area-weighted mean: −0.10 ppb), Central Europe (−0.16 ppb), and Eastern China (−0.10 ppb) (see Supplementary Table S1). In these regions, the corresponding surface ozone increases are either comparable to or smaller than the Northern Hemisphere or regional averages (see "Changes in surface ozone"). This offsetting mechanism, however, does not apply in regions with low surface NO$_x$ concentrations, such as over the oceans, the Sahara Desert, and the Arabian Peninsula (see Supplementary Fig. S1).

Mechanisms driving surface ozone reduction

As NO$_x$ emission altitude increases, so too does the transport time and therefore the amount of time for any of the ozone formed from that NO$_x$ to be destroyed. This is consistent with the monotonic reduction in area-weighted mean surface ozone response from NO$_x$ emissions at 8–10 km compared to those at 14–16 km (Fig. 1C). Emissions above 16 km lead to reductions in surface ozone, with emissions at 20–22 km causing widespread decreases across the entire Northern Hemisphere. This effect cannot be explained solely by the decay of a net ozone increase during transport, suggesting the presence of additional mechanisms driving surface ozone reduction.

The decrease in surface ozone is also unlikely to result from the downward transport of stratospheric ozone-depleted air parcels. For example, NO$_x$ emissions at 14–16 km lead to ozone depletion in the stratosphere, followed by an increase in the mid-troposphere and a subsequent decrease near the surface (Fig. 2B). In the case of NO$_x$ emissions at 20–22 km, ozone reductions are more pronounced near the surface than in the mid-troposphere (Fig. 2C), further suggesting that mechanisms beyond simple vertical transport of depleted air are at play.

Vertical pattern features (Fig. 2B) net ozone loss in the stratosphere, a "crossover" point in the upper or mid-troposphere where ozone begins to increase, and a subsequent transition near the surface where net ozone depletion reappears. This suggests a potential teleconnection between high-altitude ozone depletion and near-surface ozone reductions. The most probable explanation is that changes in column ozone affect the amount of ultraviolet (UV) light reaching the surface, including the UV radiation responsible for ozone dissociation[50]. According to the Beer–Lambert law the photolysis frequency of ozone (JO$_3$) is inversely proportional to changes in total column ozone[51]. For NO$_x$ emissions at 8–10 km, where column ozone increases, less UV radiation reaches the surface, leading to a reduction in the JO$_3$ (Fig. 2G). In contrast, emissions at 14–16 km and 20–22 km result in column ozone decreases, thereby increasing surface UV radiation and enhancing JO$_3$ (Fig. 2H, I). While relative changes in column ozone explain the direction of JO$_3$ responses, the absolute changes in JO$_3$ are largest in the tropics. This is because the photolysis frequency change is roughly proportional to the percentage change in column ozone, scaled by the baseline JO$_3$, which is inherently higher in the tropics (see Supplementary Fig. S2). Global JO$_3$ values rise by 12% Tg N^{-1} globally as a result of NO$_x$ emissions at 20–22 km, ten times higher than the increase due to emissions at 14–16 km (Fig. 2H, I). We propose that this increase in JO$_3$ is the primary factor explaining surface ozone change for higher-altitude NO$_x$ emissions, by increasing ozone loss through photolysis at the surface.

Multi-year methane feedback may also contribute to a reduction in tropospheric ozone[28,49,52]. Previous studies have explored this effect; for instance, studies reported that methane feedback enhances ozone depletion by 10%[49]. The other studies also found that global column ozone decreased by 29% due to methane feedback in a subsonic aviation scenario, while for supersonic aviation at 18–20 km, methane feedback increased net ozone depletion by 6.3%[28]. These feedbacks are included in our model and may contribute to surface ozone depletion (see "Global Chemistry Transport Model"); nonetheless, the magnitude and spatial pattern of the response indicate that the photolysis-driven mechanism is likely dominant.

We examine local correlations between ΔJO$_3$ × ozone concentration (baseline) and changes in surface ozone for emissions at 14–16 km (Fig. 3A) and 20–22 km (Fig. 3B). At emissions altitude between 14 and 16 km, the correlation coefficient between ozone loss by photolysis and surface ozone changes is −0.6. For emissions between 20 and 22 km, the correlation strengthens to −0.8. At 14–16 km, the scatter plot shows that surface ozone changes are initially positive when ozone loss by photolysis is near zero. As discussed in "Mechanisms driving surface ozone enhancement," surface ozone tends to increase in regions where ozone loss by photolysis is small (<0.01 ppmv s^{-1}), indicating the dominance of ozone-enhancing mechanisms. In contrast, for emissions at 20–22 km this ozone-enhancing influence disappears. The stronger negative correlation suggests that across grid cells, surface ozone reduction becomes more pronounced as ozone loss by

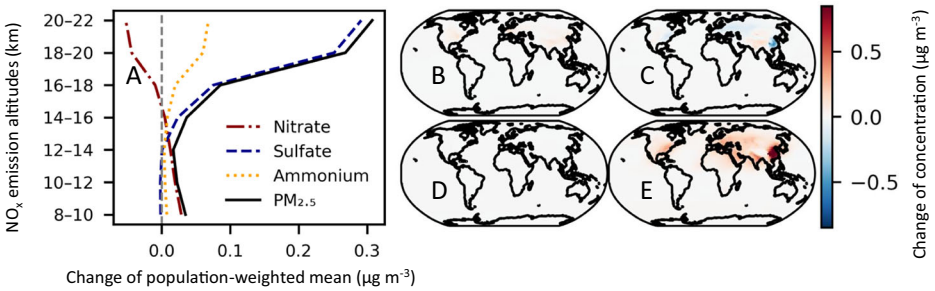


Fig. 4 | A The change in population-weighted mean $PM_{2.5}$ concentrations (μg m^{-3}) as a function of NO_x emission altitude between 30°N and 60°N. The black solid line indicates total $PM_{2.5}$, the blue dashed line indicates sulfate, the orange dotted line indicates ammonium, and the red dash-dot line indicates nitrate. **B**-**E** Show global distribution of changes in $PM_{2.5}$ components in response to NO_x emissions. **B** Change in nitrate concentrations from emissions at 8–10 km, and **C** the nitrate response from emissions at 20–22 km. **D** The sulfate response from emissions at 8–10 km, and **E** the sulfate response from emissions at 20–22 km.

photolysis increases. A possible explanation for the magnitude of this proportionality is the ozone lifetime. For downwelling air with the same absolute change in ozone, longer ozone lifetimes will mean a larger ozone concentration change at the surface[53]. This relationship helps explain the pattern shown in Fig. 1B where surface ozone reductions are larger over the ocean than over land (see "Changes in surface ozone"), likely because dry deposition is slower over the ocean (0.01–0.05 cm s^{-1}) than over land (0.05–0.8 cm s^{-1})[54,55].

Impact of NO_x emission latitude on the geographic distribution of surface ozone

The results of an evaluation of ozone produced from different sectors' NO_x emissions suggests higher ozone production efficiency in the Southern Hemisphere than in the more polluted Northern Hemisphere due to a saturation effect, where additional NO_x causes an overall reduction in the ozone production efficiency[1]. We find that the same amount of NO_x emitted at 8–10 km between the equator and 30°S produces a 24% greater global ozone burden (below 12 km) than emissions at the same altitude but between the equator and 30°N. Furthermore, the baseline area-weighted NO_x concentration in the Southern Hemisphere is 30% of that in the Northern Hemisphere. This suggests a lower likelihood of NO_x acting as a potential ozone sink in the Southern Hemisphere than in the Northern Hemisphere. We find that NO_x emissions at 8–10 km in the Southern Hemisphere result in a 2.3-fold greater response in area-weighted global surface ozone compared to equivalent emissions in the Northern Hemisphere (Fig. 1C). Nevertheless, the population-weighted global mean surface ozone changes from Southern Hemisphere emissions remains small (<0.1 ppb) (Fig. 1C). This is due to the Southern Hemisphere's lower population density and larger proportion of oceanic area, which causes a divergence between area-weighted and population-weighted responses in surface air quality to NO_x emissions (see Supplementary Fig. S3).

For higher-altitude NO_x emissions, the magnitude of the surface ozone response is larger for Northern Hemisphere emissions than for Southern Hemisphere emissions (Fig. 1C). The magnitude of surface ozone decrease is driven by changes in the ozone photolysis frequency, the background ozone concentration, and likely also the lifetime of ozone in downwelling air (see "Mechanisms driving surface ozone reduction"). The baseline annual mean area-weighted surface ozone concentration is higher in the NH (38 ppb) than in the SH (24 ppb), explaining the greater ozone loss associated with high-altitude NO_x emissions in the NH.

Changes in surface $PM_{2.5}$

NO_x emissions at 8–10 km (30–60°N) result in a $PM_{2.5}$ population-weighted mean change of 35 ng m^{-3} Tg N^{-1} (Fig. 4A), consistent with prior evaluations of air quality impacts due to subsonic aviation[14,37,56]. As emissions altitude increase from 8–10 to 12–14 km, surface $PM_{2.5}$ decreases from 35 to 17 ng m^{-3} (Fig. 4A). At higher altitudes the impact of emissions on the surface $PM_{2.5}$ increases sharply, reaching 310 ng m^{-3} Tg N^{-1} for emissions at 20–22 km (Fig. 4A), 9 times greater than the increase due to NO_x emissions at 8–10 km. In the Southern Hemisphere (Eq-30°S), NO_x emissions have a smaller impact than in the Northern Hemisphere. For emissions at 8–10 km $PM_{2.5}$ changes by −1.1 ng m^{-3}, while for emissions at 20–22 km $PM_{2.5}$ increases by 130 ng m^{-3} (see Supplementary Fig. S4).

The composition of the change in $PM_{2.5}$ varies by emission altitude. One study found that 83% of the increase in surface $PM_{2.5}$ due to subsonic aviation NO_x emissions was nitrate[3], and we too find that 83% of the change in surface $PM_{2.5}$ due to emissions at 8–10 km (30–60°N) is in the form of nitrate aerosol (Fig. 4A). However, the nitrate contributions decrease to 13% for emissions at 14–16 km, becoming negative (−17%) for emissions at 20–22 km (Fig. 4A). In contrast, sulfate contributions increase from −4% at 8–10 km to 64% at 14–16 km and 95% at 20–22 km (Fig. 4A).

The response of surface $PM_{2.5}$ to NO_x emissions exhibits regional variability. For NO_x emissions at 8–10 km, the population-weighted mean $PM_{2.5}$ increases in the nitrate component of $PM_{2.5}$ are 25 ng m^{-3} over the United States, 120 ng m^{-3} over Europe, 50 ng m^{-3} over China, and 41 ng m^{-3} over India (Fig. 4B). In contrast, for NO_x emissions at 20–22 km, the nitrate component of $PM_{2.5}$ decreases in most regions: population-weighted mean reductions are 62 ng m^{-3} over the United States, 87 ng m^{-3} over Europe, and 110 ng m^{-3} over China (280 ng m^{-3} in East China) (Fig. 4C). However, nitrate still increases over India by 43 ng m^{-3}. Sulfate components increase by 230 ng m^{-3} over the United States, 210 ng m^{-3} over Europe, 320 ng m^{-3} over India, and 540 ng m^{-3} over China (810 ng m^{-3} in East China), resulting in net $PM_{2.5}$ increases in these regions (Fig. 4E). For lower altitude NO_x emissions, Europe faces the greatest health implications due to $PM_{2.5}$ (nitrate) increases. In contrast, high altitude NO_x emissions induced nitrate reductions but stronger sulfate enhancements (Fig. 4A), resulting in the largest net population-weighted mean $PM_{2.5}$ increase (560 ng m^{-3}).

$PM_{2.5}$ driving mechanism

As for surface ozone, $PM_{2.5}$ formation also involves competing mechanisms: sulfate dominates for emissions at higher altitudes (above 14 km), while nitrate prevails when emitting at lower altitudes (below 14 km). The impact of subsonic aviation NO_x on aerosols and $PM_{2.5}$ by enhancing ozone transported to the ozone facilitates conversion of surface, non-aviation NO_x to nitrate aerosol[3,37]. Again, this ozone transport mechanism does not explain the increase in sulfate when NO_x emission altitude rises. The conversion of SO_2 to SO_4 occurs through both homogeneous and heterogeneous pathways[57]. The homogeneous, or gas-phase, oxidation is initiated by OH radicals; heterogeneous, or liquid-phase, oxidation occurs mainly through reactions with H_2O_2[58].

The depletion of stratospheric ozone resulting from NO_x emissions at 20-22 km increases UV light penetration, enhancing the ozone photodissociation frequency by 12% and increasing $O(^1D)$ production by 10% (see Supplementary Fig. S5). Accordingly, global annual average OH production increases by 10% Tg N^{-1} for emissions at 20–22 km compared to 1.4% Tg N^{-1} for emissions at 14–16 km and 0.23% Tg N^{-1} for emissions at 8–10 km (see Supplementary Fig. S6). Overall, global OH concentration increases by 13% Tg N^{-1} (emissions at 20–22 km), 2% Tg N^{-1} (14–16 km), and 1.5% Tg N^{-1} (8–10 km). At the surface, the enhanced OH radicals also

promote H_2O_2 increases of about 2% Tg N^{-1} for high altitude emissions (20–22 km), but less than 0.3% Tg N^{-1} for lower-altitude emissions (14–16 and 8–10 km). The increase in OH radicals reduces the lifetime of SO_2, promoting its conversion to SO_4 before deposition. H_2O_2 concentrations are also increased, resulting in additional liquid-phase SO_2 to SO_4 conversion although the relative increase is smaller (2% Tg N^{-1} for emissions at 20–22 km).

Our model simulations show that baseline SO_2 concentrations are greatest over the eastern United States, Europe, the Arabian Peninsula, India, and China, where we also find the greatest increases in sulfate due to high-altitude NO_x (Fig. 4E). As a result, global population-weighted mean sulfate $PM_{2.5}$ increases by 290 ng m^{-3} Tg N^{-1} for emissions at 20–22 km.

Limitations

While our simulations consistently demonstrate these altitude-dependent responses, potential source of uncertainty remain. One such uncertainty arises from variations in background at-altitude and surface NO_x which can thus influence the amount of aviation-induced ozone. For altitudes typical of subsonic aircraft (8–12 km), previous studies show that changes in surface NO_x and lightning NO_x emissions can modify the sensitivity of global ozone to aviation NO_x[59,60]. Similarly, earlier analyses demonstrated a negative correlation between background NO_y and the sensitivity of stratospheric ozone to supersonic aviation NO_x emissions[34]. However, these studies did not propagate these sensitivities to surface-level air quality, and such an analysis is considered a high priority for future research.

Another potential bias may be due to the relatively coarse resolution of our model simulations. An evaluation of global changes in surface air quality due to aviation emissions examined model resolution-dependent biases and found that simulations at a resolution roughly equivalent to 4° by 5° underestimated air quality responses by 10-20% compared to simulations at a finer (~0.5° by 0.625°) resolution[14]. Given that we perform our simulations on a 2° by 2.5° grid and are similarly simulating the effect of high-altitude emissions on air quality with similarly diffuse responses, we anticipate resolution-related biases to be less than 10% relative to simulations with grid cells an order of magnitude smaller in area.

Implications for future aviation

Our study shows that the altitude and latitude of NO_x emissions alter their impact on surface air quality. At higher altitudes, particularly above 16 km, NO_x emissions lead to a net reduction in surface ozone while increasing surface $PM_{2.5}$. In fact, emissions at 20–22 km produce up to nine times the change in surface-level $PM_{2.5}$ compared to emissions at typical subsonic cruise altitudes. This outcome indicates that regulatory limits based on surface or subsonic aircraft emissions may not be applicable for aircraft operating at higher cruise altitudes, and that there may be an additional – and as-yet unaccounted for – environmental impact of high-altitude NO_x emissions.

Our findings regarding impact mechanisms suggest that stratospheric ozone destruction from high-altitude NO_x emissions leads to increased UV radiation reaching the surface. This enhanced UV can decrease surface ozone concentrations through photolytic destruction, while simultaneously increasing surface $PM_{2.5}$ levels by accelerating the formation of sulfate aerosols. These results point to a potentially important role for surface sulfur emissions in determining the magnitude of surface $PM_{2.5}$ responses to high-altitude NO_x. They also imply the need to investigate the potential for significant surface air quality impacts resulting from high-altitude emission sources such as launch vehicles, satellite re-entry, or even geoengineering deployment platforms.

Methods

We investigate the impact of high-altitude NO_x emissions on surface air quality using a modified version of the global chemical transport model (CTM) GEOS-Chem 11-02 to simulate atmospheric chemistry, transport, and deposition processes. To examine the influence of emission altitude and latitude, we conduct 35 sensitivity simulations, 5 different emission latitudes and 7 different emission altitudes, allowing us to isolate their effects on air quality. By comparing the NO_x emissions perturbed cases with the baseline, we evaluate the impact of NO_x emissions from specific altitude and latitude bands on surface air quality. These impacts are then quantified in terms of the annual, population-weighted and area-weighted mean change in surface ozone and $PM_{2.5}$ concentrations.

Global chemistry transport model

GEOS-Chem 11-02 is a tropospheric-stratospheric 3D global CTM with 190 chemical species, 538 reactions, and 94 photolysis reactions[61]. Photolysis frequencies are computed using the FAST-JX 7.0a scheme[62]. The model incorporates key chemical families and reactions influencing ozone chemistry, such as NO_x, O_x, HO_x, halogens, and volatile organic compounds.

We conduct simulations at a global resolution of 2° latitude by 2.5° longitude. The vertical resolution corresponds to the 72 layers of the Modern-Era Retrospective analysis for Research and Applications (MERRA) meteorological data, spanning from the surface to 1 Pa (approximately 80 km altitude). To incorporate long-term methane feedbacks we conduct 14-year simulations, employing a calibrated surface methane flux instead of a fixed surface methane concentration (see below). To capture interannual variability, we use MERRA data from January 2000 to December 2011 for a 12-year simulation, followed by an additional 2 years with recycled data from 2000 and 2001. A prior study of supersonic aviation's impact using the same version of GEOS-Chem showed that after 10 years, the standard deviation of interannual variability in the ozone response had fallen to 16%[49]. The simulation results shown are averaged over the final two years.

Emission data are based on projections for 2035. We adopt an existing inventory for subsonic aviation emissions[28]. Other anthropogenic emissions are based on the IPCC Representative Concentration Pathway (RCP) 4.5 projection, while natural source emissions inventories are derived from the existing meteorological data. However, methane is treated differently in our model as we aim to capture the propagation of methane feedback due to aviation emissions. Our simulations use a calibration method[28]. First, we set the surface methane boundary condition to 1835 ppb, corresponding to the projected 2035 methane concentration under RCP 4.5. We then run one 14-year simulation to determine how much surface methane must be emitted each month to maintain the target concentration (1835 ppb). This calibrated flux is then used in place of a fixed surface concentration for all production simulations.

Earlier work evaluated ozone-related chemistry in GEOS-Chem by comparing vertical profiles of N_2O, H_2O, HNO_3, and HCl with Aura Microwave Limb Sounder observations[49]. They also evaluated the accuracy of the ozone simulation by comparing to data from the Total Ozone Mapping Spectrometer (TOMS) and Ozone Monitoring Instrument (OMI), demonstrating GEOS-Chem's ability to accurately represent ozone variability[49,61]. However, these evaluations were conducted at a global resolution of 4° latitude by 5° longitude, which may underrepresent spatial and temporal variations in atmospheric dynamics and chemistry[63]. We therefore provide an additional evaluation (see Supplementary Fig. S7) at 2° by 2.5°, demonstrating equally good performance.

Experimental design for NO_x emissions sensitivity analysis

We divide the atmosphere into 35 regions, comprising five latitudinal zones and seven altitude bands, to test changes in surface air quality based on the location of latitudinal and altitudinal NO_x. The latitudinal zones are defined as 90–60°N, 60–30°N, 30°N-Eq (equator), Eq-30°S, and 30-90°S. The 8–22 km range is divided into 2 km increments for altitude. We focus solely on latitudinal and altitudinal variations, excluding longitudinal variation. This is because zonal mixing, driven by fast-moving air currents such as the subtropical and polar jet streams, shortens zonal mixing time scales compared to meridional mixing[64–66].

In the 35 NO_x-perturbed cases, additional NO_x emissions are integrated into specific latitude and altitude regions. The emissions composition, based on mole fraction, consists of NO (90%), NO2 (9%), and HONO

(1%), consistent with aviation engine measurements[67]. A total of 3 Tg N yr^{-1} is evenly distributed across the defined latitude and altitude regions, with the same mass emitted per unit volume every day throughout the year. This emissions inventory is implemented in GEOS-Chem using the Harmonized Emissions Component (HEMCO)[68]. The NO_x-perturbed cases are compared to the baseline case to evaluate the impact of these additional NO_x emissions on the surface air quality.

Surface air quality impact metrics

We quantify surface air quality impacts by calculating the differences in surface ozone and $PM_{2.5}$ concentrations between the baseline and NO_x-perturbed cases, evaluating the impact of 3 Tg N yr^{-1} NO_x emissions at each geographical location. All results are normalized to 1 Tg N yr^{-1}. For surface air quality metrics, we evaluate each grid cell's two-year annual average change in surface ozone and $PM_{2.5}$. We compute area-weighted and population-weighted averages using the formula $X_{weighted} = \frac{\sum_i X_i w_i}{\sum_i w_i}$, where $X_{weighted}$ represents the weighted average of the air quality metrics (e.g., surface ozone or $PM_{2.5}$ change), X_i is the air quality metric at grid cell i, and w_i is the weighting factor (either the grid cell area or population). The area-weighted average estimates the global surface air quality burden change due to NO_x perturbations in each region, while the population-weighted average represents the per capita air quality impact of these perturbations. We calculate the population-weighted average using the 2015 population density data from the Gridded Population of the World, Version 4 (GPWv4)[69].

Data availability

The processed datasets required to reproduce the figures and reported values in this manuscript are available at https://github.com/lucasojs/Supersonic_Airquality/tree/main/Data. The full raw model output datasets generated during this study are not publicly archived due to their large data volume but are available from the corresponding author upon reasonable request.

Code availability

The code used during the current study, including the GEOS-Chem model code and the scripts used to generate the figures presented in this manuscript, is available at the following repository: https://github.com/lucasojs/Supersonic_Airquality/tree/main.

Received: 8 September 2025; Accepted: 6 January 2026;
Published online: 09 February 2026

References

1. Dahlmann, K., Grewe, V., Ponater, M. & Matthes, S. Quantifying the contributions of individual NO_x sources to the trend in ozone radiative forcing. *Atmos. Environ.* **45**, 2860–2868 (2011).
2. Dang, R. et al. Background nitrogen dioxide (NO_2) over the United States and its implications for satellite observations and trends: effects of nitrate photolysis, aircraft, and open fires. *Atmos. Chem. Phys.* **23**, 6271–6284 (2023).
3. Eastham, S. D. & Barrett, S. R. H. Aviation-attributable ozone as a driver for changes in mortality related to air quality and skin cancer. *Atmos. Environ.* **144**, 17–23 (2016).
4. Grobler, C. et al. Marginal climate and air quality costs of aviation emissions. *Environ. Res. Lett.* **14**, 114031 (2019).
5. Huber, D. D. E., Kort, E. A. & Steiner, A. L. Soil moisture, soil NO_x and regional air quality in the agricultural central United States. *JGR Atmos.* **129**, e2024JD041015 (2024).
6. Murray, L. T. Lightning NO_x and impacts on air quality. *Curr. Pollut. Rep.* **2**, 115–133 (2016).
7. Sheng, H. et al. Identification of NO emissions and source characteristics by TROPOMI observations – A case study in north-central Henan, China. *Sci. Total Environ.* **931**, 172779 (2024).
8. Jia, B. et al. Sensitivity of $PM_{2.5}$ to NO_x emissions and meteorology in North China based on observations. *Sci. Total Environ.* **766**, 142275 (2021).
9. Kim, S.-W. et al. Satellite-observed U.S. power plant NO_x emission reductions and their impact on air quality. *Geophys. Res. Lett.* **33**, 2006GL027749 (2006).
10. Leibensperger, E. M., Mickley, L. J., Jacob, D. J. & Barrett, S. R. H. Intercontinental influence of NO_x and CO emissions on particulate matter air quality. *Atmos. Environ.* **45**, 3318–3324 (2011).
11. Li, Y. et al. Radical chemistry and VOCs-NO_x-O_3-nitrate sensitivity in the polluted atmosphere of a suburban site in the North China Plain. *Sci. Total Environ.* **947**, 174405 (2024).
12. Monks, P. S. et al. Atmospheric composition change – global and regional air quality. *Atmos. Environ.* **43**, 5268–5350 (2009).
13. Sillman, S. The relation between ozone, NO_x and hydrocarbons in urban and polluted rural environments. *Atmos. Environ.* **33**, 1821–1845 (1999).
14. Eastham, S. D., Chossière, G. P., Speth, R. L., Jacob, D. J. & Barrett, S. R. H. Global impacts of aviation on air quality evaluated at high resolution. *Atmos. Chem. Phys.* **24**, 2687–2703 (2024).
15. Gharaylou, M., Pegahfar, N. & Alizadeh, O. The impact of lightning NO_x production on ground-level ozone in Tehran. *Earth Space Sci.* **11**, e2023EA003372 (2024).
16. Menut, L., Bessagnet, B., Mailler, S., Pennel, R. & Siour, G. Impact of Lightning NO_x emissions on atmospheric composition and meteorology in africa and europe. *Atmosphere* **11**, 1128 (2020).
17. Prashanth, P., Speth, R. L., Eastham, S. D., Sabnis, J. S. & Barrett, S. R. H. Post-combustion emissions control in aero-gas turbine engines. *Energy Environ. Sci.* **14**, 916–930 (2021).
18. Butler, T., Lupascu, A. & Nalam, A. Attribution of ground-level ozone to anthropogenic and natural sources of nitrogen oxides and reactive carbon in a global chemical transport model. *Atmos. Chem. Phys.* **20**, 10707–10731 (2020).
19. Murray, L. T., Jacob, D. J., Logan, J. A., Hudman, R. C. & Koshak, W. J. Optimized regional and interannual variability of lightning in a global chemical transport model constrained by LIS/OTD satellite data. *J. Geophys. Res.* **117**, 2012JD017934 (2012).
20. Environmental Protection Agency. 2022. Control of air pollution from aircraft engines: Emission standards and test procedures. Fed Regist. 87:72312–72391. https://www.govinfo.gov/content/pkg/FR-2022-11-23/pdf/2022-25134.pdf.
21. Gössling, S. & Humpe, A. The global scale, distribution and growth of aviation: Implications for climate change. *Glob. Environ. Change* **65**, 102194 (2020).
22. Owen, B., Lee, D. S. & Lim, L. Flying into the future: aviation emissions scenarios to 2050. *Environ. Sci. Technol.* **44**, 2255–2260 (2010).
23. Banerjee, A. et al. Lightning NO_x, a key chemistry–climate interaction: impacts of future climate change and consequences for tropospheric oxidising capacity. *Atmos. Chem. Phys.* **14**, 9871–9881 (2014).
24. Finney, D. L. et al. A projected decrease in lightning under climate change. *Nat. Clim. Change* **8**, 210–213 (2018).
25. Boom Supersonic. 2025. Overture [accessed 2025 Mar 26]. https://boomsupersonic.com/overture.
26. Boom Supersonic. 2021. United adding supersonic speeds with new agreement to buy aircraft from Boom Supersonic [accessed 2025 Mar 26]. https://boomsupersonic.com/press-release/united-adding-supersonic-speeds-with-new-agreement-to-buy-aircraft-from-boom-supersonic.
27. Dessens, O., Rogers, H. L. & Pyle, J. A. A change in the calculated impact of supersonic aircraft NO_x emissions on the atmosphere. *Aeronaut. J.* **111**, 311–314 (2007).
28. Eastham, S. D. et al. Impacts of a near-future supersonic aircraft fleet on atmospheric composition and climate. *Environ. Sci. Atmos.* **2**, 388–403 (2022).

29. Grewe, V. et al. Climate impact of supersonic air traffic: an approach to optimize a potential future supersonic fleet – results from the EU-project SCENIC. *Atmos. Chem. Phys.* **7**, 5129–5145 (2007).
30. Pitari, G. et al. Radiative forcing from particle emissions by future supersonic aircraft. *Atmos. Chem. Phys.* **8**, 4069–4084 (2008).
31. Zhang, J., Wuebbles, D. J., Kinnison, D. & Baughcum, S. L. Stratospheric ozone and climate forcing sensitivity to cruise altitudes for fleets of potential supersonic transport aircraft. *JGR Atmos.* **126**, e2021JD034971 (2021).
32. Zhang, J., Wuebbles, D. J., Pfaender, J. H., Kinnison, D. & Davis, N. Potential impacts on ozone and climate from a proposed fleet of supersonic aircraft. *Earths Future* **11**, e2022EF003409 (2023).
33. Dutta, M., Patten, K. O. & Wuebbles, D. J. Parametric analyses of potential effects on upper tropospheric/lower stratospheric ozone chemistry by a future fleet of High Speed Civil Transport (HSCT) type aircraft. NASA Contract Report NASA/CR–2005-213646 (2005).
34. Kawa, S. R. et al. Assessment of the Effects of High-Speed Aircraft in the Stratosphere. NASA Contract Report NASA/TP–1999-209237 (1995).
35. Brasseur, G. P. et al. European scientific assessment of the atmospheric effects of aircraft emissions. *Atmos. Environ.* **32**, 2329–2418 (1998).
36. Lee, D. S. et al. Transport impacts on atmosphere and climate: aviation. *Atmos. Environ.* **44**, 4678–4734 (2010).
37. Prashanth, P., Eastham, S. D., Speth, R. L. & Barrett, S. R. H. Aerosol formation pathways from aviation emissions. *Environ. Res. Commun.* **4**, 021002 (2022).
38. Derwent, R. G., Collins, W. J., Johnson, C. E. & Stevenson, D. S. Transient behaviour of tropospheric ozone precursors in a global 3-D CTM and their indirect greenhouse effects. *Clim. Change* **49**, 463–487 (2001).
39. Fuglestvedt, J. S. Climatic forcing of nitrogen oxides through changes in tropospheric ozone and methane; global 3D model studies. *Atmos. Environ.* **33**, 961–977 (1999).
40. Hodnebrog, Ø et al. Future impact of non-land based traffic emissions on atmospheric ozone and OH – an optimistic scenario and a possible mitigation strategy. *Atmos. Chem. Phys.* **11**, 11293–11317 (2011).
41. Hoor, P. et al. The impact of traffic emissions on atmospheric ozone and OH: results from QUANTIFY. *Atmos. Chem. Phys.* **9**, 3113–3136 (2009).
42. Khodayari, A., Olsen, S. C. & Wuebbles, D. J. Evaluation of aviation NO_x-induced radiative forcings for 2005 and 2050. *Atmos. Environ.* **91**, 95–103 (2014).
43. Koffi, B., Szopa, S., Cozic, A., Hauglustaine, D. & Van Velthoven, P. Present and future impact of aircraft, road traffic and shipping emissions on global tropospheric ozone. *Atmos. Chem. Phys.* **10**, 11681–11705 (2010).
44. Köhler, M. O. et al. Impact of perturbations to nitrogen oxide emissions from global aviation. *J. Geophys. Res.* **113**, 2007JD009140 (2008).
45. Stevenson, D. S. et al. Radiative forcing from aircraft NO_x emissions: Mechanisms and seasonal dependence. *J. Geophys. Res.* **109**, 2004JD004759 (2004).
46. Wild, O., Prather, M. J. & Akimoto, H. Indirect long-term global radiative cooling from NO_x emissions. *Geophys. Res. Lett.* **28**, 1719–1722 (2001).
47. Fritz, T. M. et al. Identifying the ozone-neutral aircraft cruise altitude. *Atmos. Environ.* **276**, 119057 (2022).
48. Eastham, S. D., Keith, D. W. & Barrett, S. R. H. Mortality tradeoff between air quality and skin cancer from changes in stratospheric ozone. *Environ. Res. Lett.* **13**, 034035 (2018).
49. Speth, R. L. et al. Global Environmental Impact of Supersonic Cruise Aircraft in the Stratosphere. NASA Contract Report NASA/CR-20205009400 (2021).
50. McKenzie, R. L. et al. Ozone depletion and climate change: impacts on UV radiation. *Photochem. Photobiol. Sci.* **10**, 182–198 (2011).
51. Seinfeld, J. H. & S. N. Pandis, S. N. *Atmospheric Chemistry and Physics: From Air Pollution to Climate Change* 3rd edn (Wiley, 2016).
52. Fiore, A. M. et al. Characterizing the tropospheric ozone response to methane emission controls and the benefits to climate and air quality. *J. Geophys. Res.* **113**, 2007JD009162 (2008).
53. Stevenson, D. S. et al. Multimodel ensemble simulations of present-day and near-future tropospheric ozone. *JGR Atmos.* **111**, D8 (2006).
54. Ganzeveld, L. & Lelieveld, J. Dry deposition parameterization in a chemistry general circulation model and its influence on the distribution of reactive trace gases. *J. Geophys. Res.* **100**, D10 (1995).
55. Luhar, A. K., Woodhouse, M. T. & Galbally, I. E. A revised global ozone dry deposition estimate based on a new two-layer parameterisation for air–sea exchange and the multi-year MACC composition reanalysis. *Atmos. Chem. Phys.* **18**, 4329–4348 (2018).
56. Cameron, M. A. et al. An intercomparative study of the effects of aircraft emissions on surface air quality. *JGR Atmos.* **122**, 8325–8344 (2017).
57. Saxena, P. & Seigneur, C. On the oxidation of SO_2 to sulfate in atmospheric aerosols. *Atmos. Environ.* **21**, 807–812 (1987).
58. Guo, Z. et al. Quantifying SO_2 oxidation pathways to atmospheric sulfate using stable sulfur and oxygen isotopes: laboratory simulation and field observation. *Atmos. Chem. Phys.* **24**, 2195–2205 (2024).
59. Holmes, C. D., Tang, Q. & Prather, M. J. Uncertainties in climate assessment for the case of aviation NO. *Proc. Natl. Acad. Sci. USA* **108**, 10997–11002 (2011).
60. Khodayari, A. et al. The impacts of NO_x emissions from lightning on the production of aviation-induced ozone. *Atmos. Environ.* **187**, 410–416 (2018).
61. Eastham, S. D., Weisenstein, D. K. & Barrett, S. R. H. Development and evaluation of the unified tropospheric–stratospheric chemistry extension (UCX) for the global chemistry-transport model GEOS-Chem. *Atmos. Environ.* **89**, 52–63 (2014).
62. Bian, H. & Prather, M. J. Fast-J2: Accurate Simulation of Stratospheric Photolysis in Global Chemical Models. *J. Atmos. Chem.* **41**, 281–296 (2002).
63. Strahan, S. E. & Polansky, B. C. Meteorological implementation issues in chemistry and transport models. *Atmos. Chem. Phys.* **6**, 2895–2910 (2006).
64. Allen, D. R. & Nakamura, N. A seasonal climatology of effective diffusivity in the stratosphere. *J. Geophys. Res.* **106**, 7917–7935 (2001).
65. Haynes, P. & Shuckburgh, E. Effective diffusivity as a diagnostic of atmospheric transport: 1. Stratosphere. *J. Geophys. Res.* **105**, 22777–22794 (2000).
66. Haynes, P. & Shuckburgh, E. Effective diffusivity as a diagnostic of atmospheric transport: 2. Troposphere and lower stratosphere. *J. Geophys. Res.* **105**, 22795–22810 (2000).
67. Barrett, S. R. H. et al. Guidance on the use of AEDT gridded aircraft emissions in atmospheric models. A technical note submitted to the US Federal Aviation Administration, Massachusetts Institute of Technology (MIT) (2010).
68. Keller, C. A. et al. HEMCO v1.0: a versatile, ESMF-compliant component for calculating emissions in atmospheric models. *Geosci. Model Dev.* **7**, 1409–1417 (2014).
69. Center for International Earth Science Information Network (CIESIN), Columbia University. 2017. Gridded Population of the World, Version 4 (GPWv4): Population Density, Revision 11

Acknowledgements

NO_x sensitivity simulations were conducted using the Svante cluster at the Massachusetts Institute of Technology. Meteorological data (MERRA) were provided by the Global Modeling and Assimilation Office (GMAO) at NASA Goddard Space Flight Center. This research was funded by the U.S. Federal Aviation Administration (FAA) Office of Environment and Energy through ASCENT—the FAA Center of Excellence for Alternative Jet Fuels and the

Environment—under project 58 (FAA award number 13-C-AJFE-MIT), with guidance from S. Daniel Jacob and Jeetendra Upadhyay. Publication of this manuscript was made possible by the Imperial College London Open Access Fund.

Author contributions

L.J.O. conducted the research and led the writing of the manuscript. S.D.E. supervised the research, contributed to the study design, and assisted with manuscript revisions. S.R.H.B. provided guidance and contributed to the revision of the manuscript. All authors reviewed and approved the final version of the manuscript.

Competing interests

The authors declare no competing interests.

Additional information

Supplementary information The online version contains supplementary material available at https://doi.org/10.1038/s41612-026-01324-9.

Correspondence and requests for materials should be addressed to Sebastian D. Eastham.

Reprints and permissions information is available at http://www.nature.com/reprints

Publisher's note Springer Nature remains neutral with regard to jurisdictional claims in published maps and institutional affiliations.

Open Access This article is licensed under a Creative Commons Attribution 4.0 International License, which permits use, sharing, adaptation, distribution and reproduction in any medium or format, as long as you give appropriate credit to the original author(s) and the source, provide a link to the Creative Commons licence, and indicate if changes were made. The images or other third party material in this article are included in the article's Creative Commons licence, unless indicated otherwise in a credit line to the material. If material is not included in the article's Creative Commons licence and your intended use is not permitted by statutory regulation or exceeds the permitted use, you will need to obtain permission directly from the copyright holder. To view a copy of this licence, visit http://creativecommons.org/licenses/by/4.0/.

© The Author(s) 2026